ODOVTOS
International Journal of Dental Sciences
https://revistas.ucr.ac.cr/index.php/Odontos | ISSN: 2215-3411

BASIC RESEARCH

DOI: 10.15517/IJDS.2022.49836

Received:
12-IX-2021

Accepted:
30-XI-2021

Published Online:
24-I-2022

The Effect of Curing Modes and Times of Third-Generation Led LCU on the Mechanical Properties of Nanocomposites

Efecto del modo y tiempo de fotocurado de la lámpara LCU Led de tercera generación en las propiedades mecánicas de los nanocompuestos

Burcu Oglakci DDS[1]; Rümeysa Hatice Enginler Özlen[2]; Metehan Demirkol[3]; Zümrüt Ceren Özduman DDS[4]; Bedri Onur Kucukyildirim PhD[5]; Evrim Eliguzeloglu Dalkilic DDS,PhD[6]

1. Assistant Professor, Bezmialem Vakif University Faculty of Dentistry, Deparment of Restorative Dentistry, Istanbul, Turkey. https://orcid.org/0000-0002-6587-5997
2. Restorative Dentistry Speacialist, Kısıklı mah. Nadide sk. no:17/4, Istanbul, Turkey. https://orcid.org/0000-0002-0945-5058
3. Research Assistant, Yildiz Technical University, Department of Mechanical Engineering, 34349, Istanbul, Turkey. https://orcid.org/0000-0003-4738-6476
4. Assistant Professor, Bezmialem Vakif University Faculty of Dentistry, Deparment of Restorative Dentistry, Istanbul, Turkey. https://orcid.org/0000-0003-2648-1730
5. Associate Professor, Yildiz Technical University, Department of Mechanical Engineering, 34349, Istanbul, Turkey. https://orcid.org/0000-0002-0399-5467
6. Professor, Bezmialem Vakif University Faculty of Dentistry, Deparment of Restorative Dentistry, Istanbul, Turkey. https://orcid.org/0000-0002-1075-9278

Correspondence to: Dr. Burcu Oglakci - burcu923@hotmail.com

ABSTRACT: This study evaluates the effect of curing modes and times on the mechanical properties of nanocomposites. Two nanocomposite resins were investigated: supra-nanohybrid (Estelite Posterior Quick; EP) and nanohybrid (Solare X; SX). They were polymerized with a light-emitting diode light-curing units (LED LCU, Valo) as follows: standard mode for 20s (ST20), high power mode for 12s (HP12), high power mode for 20s (HP20), extra power mode for 6s (XP6), and extra power mode for 20s (XP20). For Vickers microhardness (HV), disc-shaped specimens were fabricated (n=10). For the three-point bending test, bar-shaped specimens were fabricated (n=10). Flexural strength and resilience modulus were calculated. The fractured surfaces and specimen surfaces of composites were observed using scanning electron microscopy. The data were analyzed with repeated measures ANOVA, two-way variance, and Bonferroni tests ($p<0.05$). On the top and bottom surfaces of the EP nanocomposite resin, ST20 and HP12 revealed statistically higher HV than with XP6. Moreover, HP20

and XP20 had statistically higher HV than HP12 and XP6. For the SX nanocomposite resin, HP20 had statistically higher HV than HP12. For EP and SX, there were no significant differences in flexural strength and resilience modulus regarding the curing modes and times. Furthermore, SX demonstrated lower mechanical properties than EP. Scanning electron microscopy indicated that both nanocomposites had similar surface appearances. However, with all curing modes and times, SX exhibited layered fractures and more crack formations than EP. Different curing modes and times could influence the microhardness of nanocomposites.

KEYWORDS: LED; Nanocomposite; Microhardness; Flexural performance; Curing modes; Curing times.

RESUMEN: Este estudio evalúa el efecto del modo y tiempo de fotocurado sobre las propiedades mecánicas de los nanocompuestos. Se investigaron dos resinas nanocompuestas: supra-nanohíbrida (Estelite Posterior Quick; EP) y nanohíbrida (Solare X; SX). Se polimerizaron con unidades de fotopolimerización de diodos emisores de luz (LED LCU, Valo) de la siguiente manera: modo estándar durante 20s (ST20), modo de alta potencia durante 12s (HP12), modo de alta potencia durante 20s (HP20) , modo extra power durante 6s (XP6) y modo extra power durante 20s (XP20). Para la microdureza Vickers (HV), se fabricaron especímenes en forma de disco (n=10). Para el ensayo de flexión de tres puntos, se fabricaron probetas en forma de barra (n=10). Se calcularon la resistencia a la flexión y el módulo de resistencia. Las superficies fracturadas se observaron mediante microscopía electrónica de barrido. Los datos se analizaron con ANOVA varianza de dos vías y pruebas de Bonferroni ($p<0,05$). En las superficies superior e inferior de la resina nanocompuesta EP, ST20 y HP12 revelaron un HV estadísticamente mayor que con XP6. Además, HP20 y XP20 tenían un HV estadísticamente más alto que HP12 y XP6. Para la resina nanocompuesta SX, HP20 tenía un HV estadísticamente más alto que HP12. Para EP y SX, no hubo diferencias significativas en la resistencia a la flexión y el módulo de resistencia con respecto al modo y tiempo de fotocurado. Además, SX demostró propiedades mecánicas inferiores que EP. La microscopía electrónica de barrido indicó que ambos nanocompuestos son similares en la superficie. Sin embargo, SX exhibió fracturas en capas y más formaciones de grietas que EP. Diferentes modos y tiempos de fotocurado podrían influir en la microdureza de los nanocompuestos.

PALABRAS CLAVE: LED; Nanocompuesto; Microdureza; Flexión; Fotocurado.

INTRODUCTION

Composite resins have become the most widely used restorative material for the direct restoration of anterior and posterior teeth. These materials have been classified by their various characteristics, including the filler particle type, size, and distribution as well as the physical and mechanical properties (1). With the development of nanotechnology, nanocomposites are designed to provide maximum esthetics and superior mechanical and physical properties with reduced particle size and increased filler amount (2).

Significant improvements have been made in light-curing units (LCUs), which are used in composite resin polymerization procedures (3). In recent years, the incorporation of different photoinitiators has improved third-generation high-intensity polywave light-emitting diode (LED) LCUs (4). This device increases irradiance and claimed as it could be used for shorter exposure time to ensure adequate polymerization of composite resins (5).

Radiant exposure (J/cm²), which is the product of irradiance (mW/cm²) and exposure time (s), is considered the main factor in determining the mechanical properties of composite resins; these properties can be affected by the monomer-polymer conversion in the organic matrix (4,6). The "exposure reciprocity law" states that similar properties can be achieved as long as radiant exposure is kept constant. In other words, with a constant curing time, an increase in light irradiance can improve polymerization. Similarly, an increase in curing time with a constant light irradiance can improve polymerization. However, a single radiant exposure value cannot adequately describe or correlate with the light output spectra from a polywave LED LCU. Therefore, determining an adequate light irradiance and curing time is crucial to create a positive impact on the clinical longevity of composite resin restorations (7).

The literature provides limited data on evaluating the microhardness and flexural performance of nanocomposite resins with different curing modes and times. Peutzfeldt *et al*. (8) investigated the effect of different third-generation LED LCU curing modes and times (standard mode for 10s/20s, high power mode for 6s/12s, extra power mode for 3s/6s) on the microhardness of three dual-cured resin cement and one light-cured flowable composite resin. Moreover, they indicated that increased light irradiance and curing times improved the micromechanical properties of the resin cement. Therefore, the current study aimed to determine the effect of different third-generation LED LCU light-curing modes and times (standard mode for 20s, high power mode for 12s/20s, and extra power mode for 6s/20s) on the microhardness, flexural strength, and resilience modulus of two commercial nanocomposite resins.

The research null hypothesis is as follows:

There is no difference in the microhardness, flexural strength, and resilience modulus among different curing modes and times for nanocomposite resins.

MATERIALS AND METHODS

SAMPLE SIZE

The sample size was calculated based on the estimated effect size between groups according to the literature (9,10). It was determined that 10 samples were needed for each group to achieve a medium effect size (d=0.50) with 95% power and a 5% type 1 error rate in this study.

SPECIMEN PREPARATION

This study investigates the effect of different third-generation LCU curing modes and times on two nanohybrid composite resins: Estelite Poste-

rior Quick (EP; Tokuyama Dental Corp., Japan) and Solare X (SX; GC Corp., Japan; A2 shade). Table 1 presents the chemical compositions, batch numbers, and manufacturers of the composite resins used in this study.

A third-generation polywave LED LCU that produces high-intensity light (Valo, Ultradent, South Jordan, UT, USA; wavelength 385-515nm) was chosen. This device was used to polymerize both composite resins with the following curing modes and times:

- ST20: photopolymerized with standard mode for 20s
- HP12: photopolymerized with high power mode for 12s
- HP20: photopolymerized with high power mode for 20s
- XP6: photopolymerized with extra power mode for 6s
- XP20: photopolymerized with extra power mode for 20s

Table 2 presents the curing modes, light irradiance, curing times, and total energy density. The curing unit was held at a standardized position and distance, which was in contact with the top glass slide (11). The light irradiance was periodically controlled with a radiometer (Demetron LED Radiometer, Kerr Corp., USA). All specimen preparations were performed by a single operator, who was unaware of the type of composite resin used for the specimens (B.O.).

Table 1. The chemical compositions, batch numbers, and manufacturers of the composite resins used in this study.

Materials	Batch numbers	Chemical composition	
Estelite Posterior Quick (EP) (Tokuyama Dental Corp., Tokyo, Japan) (A2 Shade)	W123	Organic Matrix Composition: Bis-GMA, TEGDMA, Bis-MPEPP. Radical-Amplified Photopolymerization initiator technology (RAP)	Inorganic Filler Particulate: (83%wt, 70% vol) Silica-zirconia filler: 0.1-10 μm(2μm)
Solare-X (SX) (GC Corp., Tokyo, Japan) (A2 Shade)	1903042	Organic Matrix Composition: Camphorquinone photoinitiator, UDMA	Inorganic Filler Particulate: (77%wt, 65% vol) 16μm Prepolymerized fillers, 16nm silica fillers, fluoroalumino silicate glass, Lanthonid Floride fillers: 100nm (0.10μm) Inorganic fillers Silica: 850nm (0.85μm), Fumed Silica 16nm (0.016μm)

Abbreviations: 4-MET, 4-[2-(methacryloyloxy)ethoxycarbonyl] phthalic acid; 10-MDP, 10-methacryloyloxydecyl dihydrogen phosphate; BIS-GMA, bisphenol A glycidyl methacrylate; UDMA, urethane dimethacrylate; TEGDMA, triethylene glycol dimethacrylate; Bis-MPEPP, bis-methacryloxyethoxy phenyl propane.

Table 2. The curing modes, light irradiance, curing times, and total energy density used in this study.

	Curing modes	Light Irridiance (mW/cm²)	Curing time (s)	Total Energy Density (J/cm²)
ST 20	Standard	1000	20	20
HP 12	High Power	1400	12	16.8
HP 20	High Power	1400	20	28
XP 6	Xtra Power	3200	6	19.2
XP 20	Xtra Power	3200	20	64

Abbreviations: ST 20, photopolymerized with Standard Mode for 20s; HP 20, photopolymerized with High Power Mode for 20s; XP 20, photopolymerized with Xtra Power Mode for 20s; HP 12, photopolymerized with High Power Mode for 12s; XP 6, photopolymerized with Xtra Power Mode for 6.

MICROHARDNESS MEASUREMENTS

Ten disc-shaped specimens of each composite resin (diameter: 4mm, height: 2mm) were fabricated using a Teflon mold at each curing mode and time (12). Both composite resins were inserted into the mold in a single increment and covered on both sides with a transparent polyester matrix strip (Mylar Strip, SS White Co., Philadelphia, PA, USA) and a glass slide. The mold was compressed using two glass slides to remove the excess material. Then, the specimens were polymerized through the top glass slide with the LED LCU (5) and divided into five groups to the curing modes and times (n=10). The specimens were removed from the mold after polymerization, and the bottom surfaces were marked with a permanent marker. They were kept in distilled water at 37°C for 24h in a dark vial (9). The specimens were subjected to Vickers microhardness testing with an HMV Microhardness Tester (HMV-G, Shimadzu Corp., Japan). All microhardness testing procedures were conducted according to the ASTM E384-17 standard. This standard required all tests to be applied at a load of 200 g with a 10s dwell time on the top and bottom surfaces (13). The parameters for applied load and dwell time were selected following the specified limits stated in the standard. A load value of 200 g was selected to simplify locating and measuring indentations with the light microscope embedded into the microhardness testing device. A dwell time of 10s was selected to provide the material with enough elastic recovery time. A second operator, who was unaware of the type of composite resin or the type of polymerization procedures, performed all of the microhardness measurements (R.H.Ö.).

FLEXURAL STRENGTH (FS) AND RESILIENCE MODULUS (RM) MEASUREMENTS

A total of 100 bar-shaped specimens (2×2×25mm) were fabricated using a half-split stainless steel mold, following ISO 4049, for each composite resin (N=50/composite; 14). Both composite resins were inserted into the mold in a single increment and covered on both sides with a transparent polyester matrix strip and a glass slide. The specimens were polymerized through the top glass slide with the LED LCU and divided into five groups as mentioned above (n=10). The polymerization of the composite resins was performed in three separate overlapping parts from both sides of the mold. The specimens were stored in distilled water at 37°C for 24h in a dark vial before testing (14). Then, a three-point bending test was performed using a universal testing machine (AGS-X, Shimadzu Corp., Japan) at a cross-head speed of 1.0 mm/min until the specimen fractured (span length of 15mm). The load-deflection curves were recorded with analysis software (Trapezium X, Shimadzu Corp., Japan). The FS was calculated automatically by the software using Equation 1.

$$FS=3FL/(2wt^2) \quad \text{(Eq.1) (15)}$$

In the above equation, F is the ultimate force, L is the length between supports, w is the width, and t is the thickness of the specimen.

The RM was calculated using Equation 2.

$$RM=1/2\ (FS).\varepsilon \quad \text{(Eq. 2) (15)}$$

In Equation 2, ε is the strain derived from the obtained stress-strain curve as the maximum deformation. A second operator, who was unaware of the type of composite resin or the type of polymerization procedures, performed the three-point bending test (R.H.Ö.). All derivations and calculations were realized.

SCANNING ELECTRON MICROSCOPE ANALYSIS

The specimens were sputter-coated with gold to prevent the charging effect and provide fine imaging. Then, after the three-point bending test, the specimens' surfaces were examined using scanning electron microscopy (SEM; Phenom XL, Thermo Fisher Scientific, USA) imaging at 400x and 1000x magnifications, using 15 kV and 10 kV accelerating voltages, respectively. An operator, who was unaware of the type of curing mode, time, and composite that was used, performed all the SEM analyses (M.D.).

STATISTICAL ANALYSIS

Statistical analysis was performed using SPSS 22.0 for Windows (SPSS Inc., Chicago, IL, USA). Microhardness data were first analyzed for normality of variables using the Shapiro-Wilk test, and Levene's test was used to indicate the homogeneity of variances. These data were normally distributed. Repeated-measures ANOVA was used to compare the data within groups and between groups. Post hoc comparisons were performed with the Bonferroni test. The Shapiro-Wilk test was used to analyze FS and RM data to identify variable normality. The Box's M test was used to indicate the homogeneity of variances. These data were normally distributed. Additionally, two-way variance analysis was used to compare the differences within and between groups. Statistical significance was determined at a confidence level of 0.05 in all analyses.

RESULTS

MICROHARDNESS MEASUREMENTS

Table 3 presents the mean HV values of the curing modes and times used on the composites. On the top and bottom EP surfaces, the HV values of the XP6 curing mode were statistically lower than those of ST20 and HP12 ($p<0.05$). However, there were no significant differences in the HV values between ST20 and HP12 ($p>0.05$). When comparing curing times, it was found that the HV values on the top and bottom EP surfaces of HP20 were statistically higher than HP12 and the HV values of XP20 were statistically higher than XP6 ($p<0.05$). For the curing modes used on the top and bottom SX surfaces, there were no significant differences in HV between ST20, HP12, and XP6 ($p>0.05$). Regarding the curing times for the top and bottom SX surfaces, the HV values of HP20 were statistically higher than HP12 ($p<0.05$), and there were no significant differences in HV between XP20 and XP6 ($p>0.05$). When comparing the composite resins, at the top and bottom surfaces the HV values of SX were statistically lower than EP in terms of all curing modes and times ($p<0.05$).

Table 3. The mean microhardness values (HV) of the curing modes and times used for each composite (N/mm2).

		ST 20	HP 12	HP 20	XP 6	XP 20	*p*
EP	Top	91.6±7.68[a]	89.20±7.18[a]	103.57±5.60[b]	79.28±6.70[c]	96.89±7.48[a b]	0.012
	Bottom	82.52±5.92[a]	83.20±6.59[a]	100.98±5.23[b]	61.99±4.46[c]	95.10±11.42[b]	<0.001
SX	Top	32.7±1.29[a b]	27.86±1.15[a]	36.03±1.75[b]	31.66±4.39[a b]	32.48±4.23[a b]	0.023
	Bottom	29.77±1.38[a b]	27.18±0.86[a]	35.09±2.86[b]	27.86±5.02[a]	31.54±1.69[a b]	<0.001
P values between SX and EP	Top	<0.001	<0.001	<0.001	<0.001	<0.001	
	Bottom	<0.001	<0.001	<0.001	<0.001	<0.001	

* Different superscript small letters indicate the significant differences within the same row (p<0.05).
Abbreviations: SX, Solare X; EP, Estelite Posterior Quick; ST 20, Standard Mode for 20 s; HP 20, High Power Mode for 20 s; XP 20, Xtra Power Mode for 20 s; HP 12, High Power Mode for 12 s; XP 6, Xtra Power Mode for 6 s.

FLEXURAL STRENGTH (FS) AND RESILIENCE MODULUS (RM) MEASUREMENTS

The mean FS and RM values of the different curing modes and times for each composite are presented in Figure 1 and Figure 2, respectively. For EP and SX, concerning the curing modes and times, there were no significant differences in FS and RM (p>0.05). However, for EP, the FS values with HP20 were statistically higher than ST20 (p<0.05).

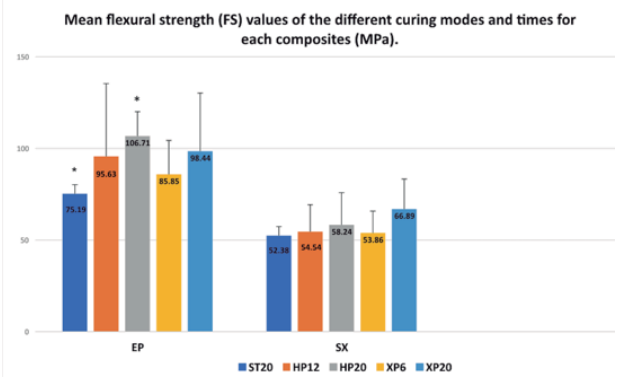

Figure 1. The mean flexural strength (FS) values of the curing modes and times used for each composite (MPa).
*There were significant differences in standard deviations for Estelite Posterior Quick (EP; p<0.05).
Abbreviations: SX, Solare X; EP, Estelite Posterior Quick; ST 20, Standard Mode for 20s; HP 20, High Power Mode for 20s; XP 20, Xtra Power Mode for 20s; HP 12, High Power Mode for 12s; XP 6, Xtra Power Mode for 6s.

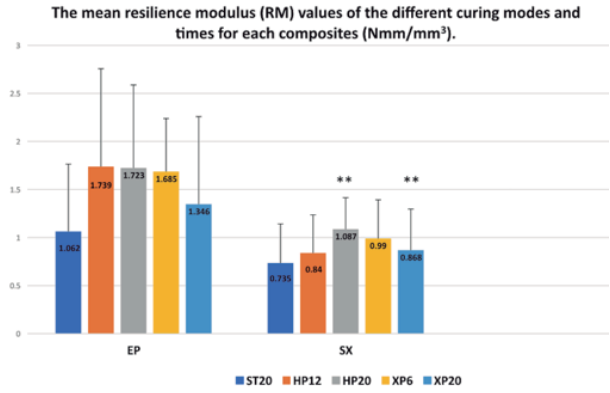

Figure 2. The mean resilience modulus (RM) values of the curing modes and times used for each composite (Nmm/mm3).** There were significant differences in standard deviations for Solare X (SX; p<0.05).
Abbreviations: SX, Solare X; EP, Estelite Posterior Quick; ST 20, Standard Mode for 20s; HP 20, High Power Mode for 20s; XP 20, Xtra Power Mode for 20s; HP 12, High Power Mode for 12s; XP 6, Xtra Power Mode for 6s.

When comparing the composite resins, the data indicates that SX has statistically lower FS than EP with all curing modes and times. Furthermore, the data suggest that SX has statistically lower RM than EP with HP20, HP12, and XP6 (p<0.05).

SCANNING ELECTRON MICROSCOPE ANALYSIS

Figure 3 presents representative SEM images of fractured surfaces with the different

curing modes and times for each composite. EP with HP20 and HP12 revealed lamellar fractures and pores (Figure 3.b and Figure 3.c), while ST20 and XP20 presented relatively smoother surfaces (Figure 3.a and Figure 3.e). When comparing the composite resins with all curing modes and times, SX demonstrated different types of filler particles and exposed large fillers, pores, and layered fractures than EP. Additionally, SX exhibited similar fractured surface appearances for all tested groups (Figure 3.f-Figure 3.j). However, more layer separation was found for SX with ST20 (see Figure 3.f).

Figure 4 displays representative SEM images of specimen surfaces with the different curing modes and times for each composite. When comparing the specimen surfaces for the curing modes and times, SX with XP20 and ST20 exhibited more crack formations on the surfaces. Furthermore, ST20 caused crack propagation in larger areas than XP20 (Figure 4.f and Figure 4.j). Comparison between the composite resins with all curing modes and times reveals that SX demonstrated increased and deeper crack formations than EP.

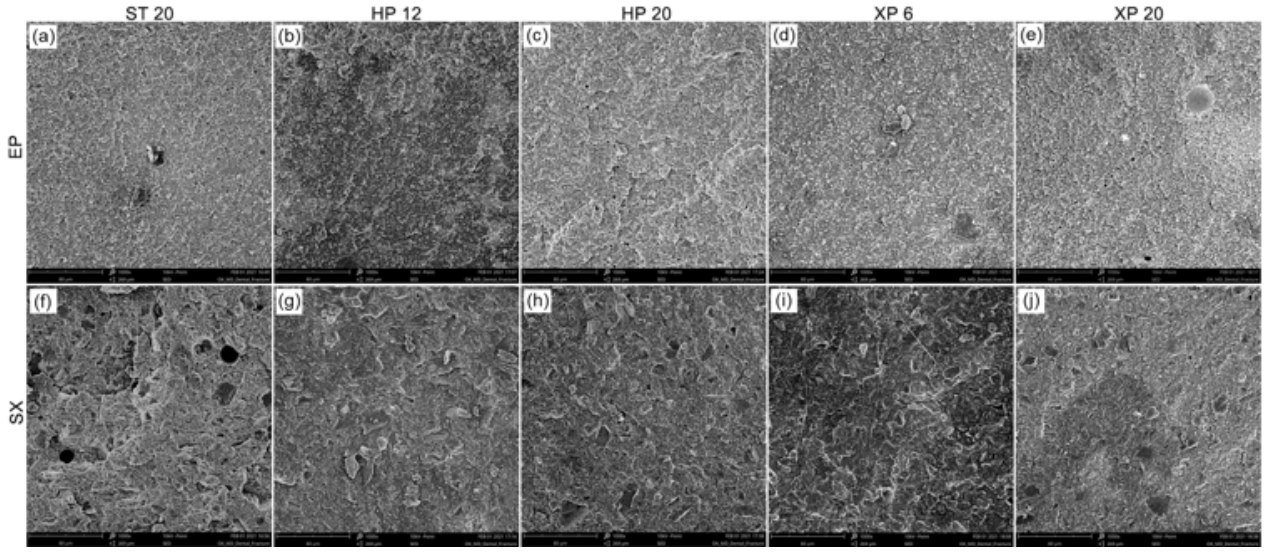

Figure 3. The scanning electron microscopy (SEM) images of fractured surfaces with the curing modes and times used for each composite (original magnification 1000X).
Abbreviations: SX, Solare X; EP, Estelite Posterior Quick; ST 20, Standard Mode for 20s; HP 20, High Power Mode for 20s; XP 20, Xtra Power Mode for 20s; HP 12, High Power Mode for 12s; XP 6, Xtra Power Mode for 6s.

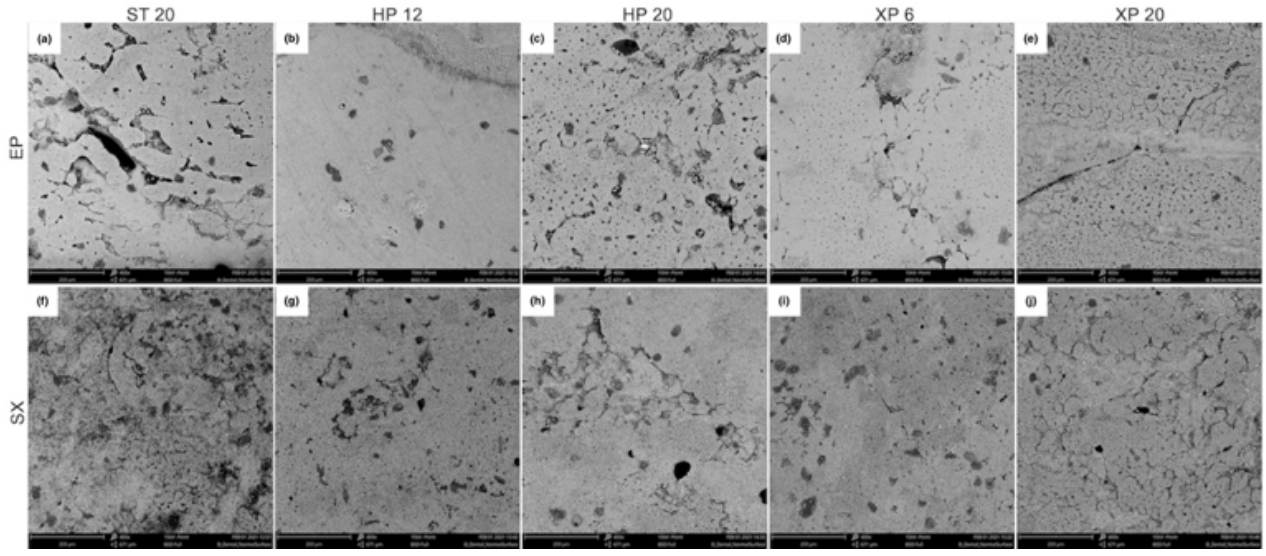

Figure 4. The scanning electron microscopy (SEM) images of specimen surfaces with the curing modes and times used for each composite (original magnification 400X).
Abbreviations: SX, Solare X; EP, Estelite Posterior Quick; ST 20, Standard Mode for 20s; HP 20, High Power Mode for 20s; XP 20, Xtra Power Mode for 20s; HP 12, High Power Mode for 12s; XP 6, Xtra Power Mode for 6s.

DISCUSSION

The critical issue is determining the total energy density (J/cm²) needed to achieve proper polymerization of the composite resin restorations (16). A given total energy density can be delivered with different combinations of light irradiance and curing time (17). The exposure reciprocity law or "total energy principle" was generally corroborated. It indicated that at a certain radiant exposure, all combinations of irradiance and exposure duration result in comparable material properties, such as the degree of double bond conversion, hardness, and flexural properties (17,18). However, it is generally well-known that it is better to overexpose a restoration rather than underexposure it, noting that thermal effects can be significant for long curing times (19). This study investigated the applicability of the exposure reciprocity law for nanocomposite polymerization using a third-generation LED LCU. This type of LED LCU has properties that prevent wavelength-incompatibility issues, such as higher light irradiance; different curing modes (standard, high power, extra power, turbo, or soft-start); and polywave (dual/multipeak) technology (11). Furthermore, the study tested two commercial nanocomposite resins (supra-nanohybrid and nanohybrid composites), which differed in photoinitiating systems and the filler type, size, and amount. Ultimately, the study evaluated the effect of LED LCU curing modes and times on the microhardness, flexural strength, and resilience modulus of nanocomposite resins. Based on the results of this study, the hypothesis, which proposed that there would be no difference in microhardness, flexural modulus, and resilience modulus among different curing modes and times for nanocomposite resins, was partially rejected.

Surface hardness, which is dependent not only on the effectiveness of polymerization but also on the nature of bonding between monomers, is one of the most important mechanical properties of composite resins for posterior stress-bearing areas (20). As light passes through the composite resins, light absorption and attenuation reduce the light intensity (21). The literature reports that the effectiveness of polymerization is inversely proportional to the filler amount, owing to decreased light transmission. Moreover, light

scattering from smaller filler particles has been found to reduce the effectiveness of polymerization because of the difference in refractive indices between the filler and the matrix resin (22). In this study, when comparing the curing modes on the top and bottom surfaces for nanohybrid composite resins, no significant differences in HV were observed. For supra-nanohybrid composites, photopolymerization with XP6 caused significantly lower HV than with ST20 and HP12. Nanohybrid composite resin has a lower filler amount and larger filler particle sizes than supra-nanohybrid composite, resulting in restorative material that is more translucent, allowing light transmission. This finding concerning a supra-nanohybrid composite and curing modes can be explained by the fact that higher light irradiance with shorter exposure time (XP6) may lead to insufficient photopolymerization due to the higher inorganic filler amount and smaller filler particles, which increases light attenuation (scattering). Gonulol *et al*. (23), who evaluated the effect of different curing modes on the microhardness of microhybrid composites, giomers, compomers, and resin-modified glass ionomers, reported that all restorative materials exhibited lower microhardness at both surfaces after photopolymerization with XP6 when compared to HP12 and ST20.

The frequently used composite resin photoinitiators are based on camphorquinone (CQ). However, while CQ alone can start polymerization, the reaction would occur at a low rate (4). Radical amplified photopolymerization technology was introduced as a method to reduce the amount of CQ by using an innovative co-activator (9). In this study, when comparing the curing times, the top and bottom surfaces of nanohybrid photopolymerization with HP20 had significantly higher HV than HP12. However, no significant differences were observed between XP20 and XP6. The photopolymerization with XP6 could have provided higher light irradiance (3200 mW/cm^2) for a shorter exposure time, and this energy density might be considered to be effective on increased microhardness. On top and bottom surfaces of supra-nanohybrid composite resins, photopolymerization with HP20 caused significantly higher HV than HP12. Additionally, XP20 resulted in significantly higher HV than XP6. For supra-nanohybrid composite resin, the finding of increased microhardness with increased curing time aligns with previous studies that state that prolonged curing time might be required for radical amplified photopolymerization technology use with this type of composite resin (9). Lima *et al*. (24) evaluated the microhardness of nano filled composites with LED LCU (800 mW/cm^2) for two different curing times (20s and 40s). They suggested that the increased polymerization time increased the microhardness of the nano filled composites on the top and bottom surfaces.

In this study, when comparing the microhardness of composite resins, the HV of top and bottom surfaces of the supra-nanohybrid composite were found to be significantly higher than those of the nano-hybrid composite, regardless of curing modes or times. This can be attributed to the higher filler amount of the supra-nanohybrid composite (83% wt, 70% vol) when compared to that of the nanohybrid composite (77% wt, 65% vol). It was reported that inorganic filler particles and microhardness values are positively correlated, given that a decrease in filler amount results in reduced mean hardness values (25).

Flexural strength (FS) is the maximum stress, such as chewing loads, that a material can withstand before failure, and FS can be used as an indicator of a restorative material's durability under stress (26). In this study, when comparing the curing modes for the nanohybrid and supra-nanohybrid composites, ST20 resulted in similar FS to HP12 and XP6. No significant differences in FS were found among the curing times. However, Peutzfeldt and Asmussen (17), who studied the energy density (light irradiance and exposure time)

of a quartz-tungsten-halogen light source, reported that composite resins obtained higher FS with increased total energy density. They also indicated that higher light irradiance and shorter exposure time decreased FS.

Flexural properties can be affected by filler size, morphology, and the restorative material filler amount. A higher filler amount and smaller spherical-shaped filler provide a higher packing density and generally improved mechanical properties (27). Nonetheless, it has been reported that other factors can impact FS, such as stress transfer between the filler particles and matrix and adhesion between these components (28). When comparing the composite resins, photopolymerized with all curing modes and times, the nanohybrid composite displayed significantly lower FS than the supra-nanohybrid composite. This finding can be attributed to the lower filler amount and fluoroaluminosilicate glass fillers of the nanohybrid composite. The prepolymerized fillers of the nanohybrid composite resin were not well bonded to the polymer matrix (29). Additionally, there may be differences in the adhesion between the filler particles and matrix among these composite resins.

Resilience modulus (RM) is defined as a restorative material's ability to absorb energy when it is elastically deformed from external stress before failure. Therefore, a high RM is required for a restoration's long-term stability (30). In this study, no significant differences in RM were found between both composite resins, polymerized with all curing modes and times. However, despite no statistically significant differences, XP6 caused higher resilience than XP20. A decrease in the amount of energy absorbed might occur due to excessive embrittlement after photopolymerization with XP20. Consequently, the high total energy density obtained with XP20 resulted in decreased resilience and increased brittleness.

Observation of the SEM micrographs of the supra-nanohybrid composite fractured surfaces revealed that HP20 (Figure 3.c) and HP12 (Figure 3.b) created lamellar fractures, while ST20 (Figure 3.a) created a smoother surface appearance. However, there were no significant differences in FS and RM. For the nanohybrid composite resin, all curing times and modes caused a similar appearance. Therefore, the SEM observations confirmed the FS and RM findings of this study. By comparison, separated layers were observed after polymerization with ST20 (Figure 3.f). Regarding the composite resins, all the specimens broke with an apparent brittle behavior with all curing modes and times. Damaged large glass fillers were exposed, less matrix was visible, and more pores and layered fractures were dominant for the nanohybrid composite resin. Oppositely, smoother surface appearances were noted for the supra-nanohybrid composite. The SEM observations validate that the supra-nanohybrid composite has a strong interface between the fillers and the matrix. Exclusive spherical-shaped fillers and an increased supra-nanohybrid composite filler amount better facilitated the load transmission in the restoration than the nanohybrid composite with irregularly shaped fillers; this occurred since mechanical stresses tend to concentrate on the protuberances of the nanohybrid composite's filler particles (27). Additionally, the nanohybrid composite's prepolymerized filler particles were not well bonded to the polymer matrix. The resin fillers are heat cured and do not form covalent chemical bonds with the polymerizing matrix due to the lack of available methacrylate groups on their surfaces. Therefore, they become unbonded and dislodged under high stresses (31).

Observations of the SEM micrographs of the nanohybrid composite specimen surfaces revealed that XP20 (Figure 4.j) and ST20 (Figure 4.f) created more crack formations on the surfaces than other

tested curing modes and times. However, crack propagation in larger areas were detected with ST20. For both composites, XP6 (Figure 4.d and Figure 4.i) did not negatively affect the surface properties through high irradiance with shorter exposure. Furthermore, with all curing modes and times, more crack formations and rougher surfaces were noted for the nanohybrid composite than for the supra-nanohybrid composite since the increased filler particles of the supra-nanohybrid composite improved the fracture energy and created a pinning effect in the propagation of cracks (32).

CONCLUSION

The present study concludes that different curing modes and times can influence the mechanical properties of nanocomposites, such as HV. The nanohybrid composite resin exhibited lower mechanical properties than the supra-nanohybrid composite resin. The SEM observations indicated that both composite resins exhibited similar surface appearances with all curing modes and times. However, the nanohybrid composite resin displayed layered fractures and more crack formations than the supra-nanohybrid composite resin. It was found that the high total energy density obtained with XP20 increased embrittlement and decreased the amount of energy absorbed during restoration.

AUTHOR CONTRIBUTION STATEMENT

Conceptualization and design: B.O., Z.C.O., B.O.K., E.E.D.
Literature review: B.O.
Methodology and validation: B.O.
Formal analysis: B.O.
Investigation and data collection: B.O., R.H.E.O., M.D.
Data analysis and interpretation: B.O., B.O.K., E.E.D.
Writing: B.O., Z.C.O.
Review & editing: Z.C.O., B.O.K., E.E.D.

DISCLOSURE STATEMENT

The authors do not have any financial interest in the companies whose materials are included in this article.

ACKNOWLEDGEMENTS

Many thanks to Assistant Professor Sevilay Karahan for her help with statistical analyses and Yildiz Technical University Advanced Materials Research Group (YTU-AMRG) for all contributions they made in the course of the study. This study was co-funded by Tokuyama Dental Corp (Tokyo, Japan) and GC Europe (Leuven, Belgium). The funders had no role in the design, conduct, evaluation, or interpretation of the study, or in writing the manuscript.

REFERENCES

1. Demarco F.F., Corrêa M.B., Cenci M.S., Moraes R.R., Opdam N.J. Longevity of posterior composite restorations: not only a matter of materials. Dent Mater. 2012; 28 (1): 87-101.
2. Subrahami K., Ahmed W. Emerging nanotechnologies in dentistry-materials, processes and applications Waltham (MA): Elsevier Inc. 2012.
3. Jandt K.D., Mills R.W. A brief history of LED photopolymerization. Dent Mater. 2013; 29 (6) 605-617.
4. Jakubiak J., Allonas X., Fouassier J., Sionkowska A., Andrzejewska E., Linden L. Camphorquinone-amines photoinitating systems for the initiation of free radical polymerization. Polymer 2003; 44 (8): 5219-5226.
5. Randolph L.D., Palin W.M., Bebelman S., Devaux J., Gallez B., Leloup G. Ultra-fast light-curing resin composite with increased conversion and reduced monomer elution. Dent Mater 2014; 30 (5): 594-604.

6. Platt JA, Price RB. Light curing explored in Halifax. Oper Dent 2014; 39 (6):561-563.
7. Feng L., Suh BI. Exposure reciprocity law in photopolymerization of multi-functional acrylates and methacrylates. Macromol Chem Phys 2007; 208 (3): 295-306.
8. Peutzfeldt A., Lussi A., Flury S. Effect of High-Irradiance Light-Curing on Micro-mechanical Properties of Resin Cements. Biomed Res Int. 2016; 4894653. doi: 10.1155/2016/4894653
9. Ilie N, Kreppel I, Durner J. Effect of radical amplified photopolymerization (RAP) in resin-based composites. Clin Oral Investig. 2014; 18 (4): 1081-1088.
10. Shibasaki S., Takamizawa T., Nojiri K., Imai A., Tsujimoto A., Endo H., et al. Polymerization Behavior and Mechanical Properties of High-Viscosity Bulk Fill and Low Shrinkage Resin Composites. Oper Dent. 2017; 42 (6): E177-E187. doi: 10.2341/16-385-L
11. Gan J.K., Yap A.U., Cheong J.W., Arista N., Tan C.B.K. Bulk-Fill Composites: Effectiveness of Cure With Poly- and Monowave Curing Lights and Modes. Oper Dent. 2018; 43 (2): 136-143. doi: 10.2341/16-304-L
12. Yap A.U.J., Seneviratne C. Influence of light energy density on effectiveness of composite cure. Oper Dent. 2001; 26 (5): 460-6.
13. Özduman Z.C., Kazak M., Fildişi M.A., Özlen R.H., Dalkilic E., Donmez N. Effect of Polymerization Time and Home Bleaching Agent on the Microhardness and Surface Roughness of Bulk-Fill Composites: A Scanning Electron Microscopy Study, Scanning 2019.:2307305. doi: 10.1155/2019/2307305
14. ISO-Standards 2009. ISO 4049 Dentistry-Polymer-Based Restorative Materials Geneve: International Organization for Standardization.
15. Askeland DR. The Science and Engineering of Materials, Springer Science+Business Media, New York. 1996 Online ISBN: 978-1-4899-2895-5 https://doi.org/10.1007/978-1-4899-2895-5
16. Yap A.U.J., Seneviratne C. Influence of light energy density on effectiveness of composite cure. Oper Dent. 2001; 26 (5): 460-6
17. Peutzfeldt A., Asmussen E. Resin Composite Properties and Energy Density of Light Cure. J Dent Res. 2005; 84 (7): 659-62.
18. Price R.B.T., Felix C.A., Andreou P. Effects of resin composite composition and irradiation distance on the performance of curing lights. Biomaterials 2004; 25 (18): 4465-4477, 2004.
19. Rueggeberg F.A., Giannini M., Arrais C.A.G., Price R.B.T. Light curing in dentistry and clinical implications: a literature review. Braz Oral Res. 2017; 31 (Supplement 1) e61.
20. Borges B.C.D., Groninger A.I.S., Soares G.P., Santos-Daroz C.B.D., Ambrosano G.M.B., Marchi GM. Curing quality of composites as influenced by the filler content, light source and curing time. Dentistry 2012; 1 (1): 103.
21. Price R.B.T. Light curing in dentistry. Dent Clin N Am. 2017; 61 (4): 751-778.
22. Bouschlicher M.R., Rueggeberg F.A., Wilson B.M. Correlation of bottom-to-top surface microhardness and conversion ratios for a variety of resin composite compositions. Oper Dent. 2004; 29 (6): 698-704.
23. Gonulol N., Ozer S., Tunc E.S. Effect of a third-generation LED LCU on microhardness of tooth-colored restorative materials. Int J Pediatr Dent. 2016; 26(5): 376-82
24. Lima A.F., de Andrade K.M.G., da Cruz Alves L.E., Sores G.P., Marchi G.M., Aguiar

F.H.B. Influence of light source and extended time of curing on microhardness and degree of conversion of different regions of a nanofilled composite resin. Eur J Dent. 2012; 6 (2): 153-157.

25. Kim K.H., Ong J.L., Okuno O. The effect of filler loading and morophology on the mechanical properties of contemporary composites. J Prosthet Dent. 2002; 87 (6): 642-94.
26. Heintze S.D., Zimmerli B. Relevance of in vitro tests of adhesive and composite dental materials, a review in 3 parts. Part 1: approval requirements and standardized testing of composite materials according to ISO specifications. Schweiz Monatsschr Zahnmed 2011; 121(9): 804-816
27. Goracci C., Cadenaro M., Fontanive L., Giangrosso G., Juloski J., Vichi A. Polymerization efficiency and flexural strength of low-stress restorative composites. Dent Mater. 2014; 30 (6): 688-694.
28. Chung S.M., Yap A.U.J., Chandra S.P., Lim CT. Flexural Strength of Dental Composite Restoratives: Comparison of Biaxial and Three-Point Bending Test. J Biomed Mater Res. 2004; 71(2): 278-83.
29. Par M., Tarle Z., Hickel R., Ilie N. Mechanical properties of experimental composites containing bioactive glass after artificial aging in water and ethanol. Clin Oral Investig. 2019; 23(6): 2733-2741. doi: 10.1007/s00784-018-2713-6. Epub 2018 Oct 25.
30. Salazar D.C., Dennison J., Yaman P. Inorganic and prepolymerized filler analysis of four resin composites. Oper Dent. 2013; 38 (6): E201-209. doi: 10.2341/12-474-L
31. Boussèsa Y., Brulat-Bouchardb N., Boucharda P.O., Abouelleilc H. & Tilliera Y. (2020) Theoretical prediction of dental composites yield stress and flexural modulus based on filler volume ratio Dental Materials 36 (1) 97-107. doi: 10.1016/j.dental.2019.10.012